

Modified Peptides as Potent Inhibitors of the Postsynaptic Density-95/*N*-Methyl-D-Aspartate Receptor Interaction

Anders Bach,[†] Celestine N. Chi,[‡] Thomas B. Olsen,[†] Søren W. Pedersen,[†] Martin U. Røder,[†] Gar F. Pang,[†] Rasmus P. Clausen,[†] Per Jemth,[‡] and Kristian Strømgaard^{*†}

Department of Medicinal Chemistry, The Faculty of Pharmaceutical Sciences, University of Copenhagen, Universitetsparken 2, DK-2100 Copenhagen, Denmark, and Department of Medical Biochemistry and Microbiology, Uppsala University, BMC, Box 582, S-75123 Uppsala, Sweden

Received July 9, 2008

The protein–protein interaction between the NMDA receptor and its intracellular scaffolding protein, PSD-95, is a potential target for treatment of ischemic brain diseases. An undecapeptide corresponding to the C-terminal of the NMDA was used as a template for finding lead candidates for the inhibition of the PSD-95/NMDA receptor interaction. Initially, truncation and alanine scan studies were carried out, which resulted in a pentapeptide with wild-type affinity, as examined in a fluorescence polarization assay. Further examination was performed by systematic substitutions with natural and unnatural amino acids, which disclosed a tripeptide with micromolar affinity and *N*-methylated tetrapeptides with improved affinities. Molecular modeling studies guided further *N*-terminal modifications and introduction of a range of *N*-terminal substitutions dramatically improved affinity. The best compound, *N*-cyclohexylethyl-ETAV (**56**), demonstrated up to 19-fold lower K_i value ($K_i = 0.94$ and $0.45 \mu\text{M}$ against PDZ1 and PDZ2 of PSD-95, respectively) compared to wild-type values, providing the most potent inhibitors of this interaction reported so far. These novel and potent inhibitors provide an important basis for development of small molecule inhibitors of the PSD-95/NMDA receptor interaction.

Introduction

Protein–protein interactions (PPIs^a) are essential to vital cellular processes such as signal transduction, hormone–receptor interactions, and programmed cell death. Hence, PPIs are also involved in numerous pathophysiological states and serve as potential targets for therapeutic intervention.^{1,2} However, PPIs have generally been perceived as difficult to target with small organic molecules because they are often characterized by large, flat, and hydrophobic interfaces.³ This perception is changing, as it has been realized that often only a few amino acids on the protein surface are essential for interaction,^{4–6} and recently, a number of small molecule inhibitors of PPIs have been published.^{4,7–9}

An interesting class of PPIs is the one involving PDZ domains. PDZ domains often function as modules in scaffolding proteins that are involved in assembling large protein complexes in the cell^{10,11} and are highly abundant in eukaryotic organisms.¹² PDZ domains comprise about 90 amino acids and generally interact with only a few amino acids of the C-terminal part of the interacting protein.^{13–15} The peptide-binding specificity of PDZ domains has been thoroughly investigated, and PDZ domains are typically divided into three classes according to the sequence of their ligands.¹⁵ However, recent investigations demonstrate a more even distribution in selectivity space rather than segregation into isolated groups.^{16,17} PSD-95, which is studied here, contains three PDZ domains, PDZ1–3, which bind

peptide ligands with the consensus sequence Glu/Gln-Ser/Thr-X-Val-COOH, thus being designated class I PDZ domains.^{15,18,19}

The structural basis for the interaction of PDZ domains with C-terminal peptides was first elucidated by an X-ray crystallographic structure of PDZ3 of PSD-95 in complex with a native peptide ligand, CRIPT.²⁰ PDZ3 contains six antiparallel β -strands (βA – βF) and two α -helices (αA and αB), and the C-terminal peptide ligand binds as an additional antiparallel β -strand into a groove between the βB strand and αB helix.²¹ Two residues in the peptide ligand are considered particularly important for affinity and specificity, the first (P^0) and the third (P^{-2}) amino acids (counting from the C-terminal). The side chain of the amino acid in P^0 position projects into a hydrophobic pocket and amino acids with aliphatic side chains (Val, Ile, and Leu) is required.¹⁵ In the PDZ3–CRIPT structure, the hydroxyl oxygen of Thr (P^{-2}) forms a hydrogen bond with the nitrogen of the imidazole side chain of His372,²⁰ which is a highly conserved residue in class I PDZ domains. The importance of His372 has been corroborated by mutagenesis studies.²² A conserved Gly-Leu-Gly-Phe (positions 322–325 in PDZ3) motif and a positively charged residue (Arg318 in PDZ3) of PDZ domains mediate binding to the C-terminal carboxylate group.^{20,22}

The PDZ1 and PDZ2 domains of PSD-95 interact with a number of proteins including a group of ionotropic glutamate receptors, the *N*-methyl-D-aspartate (NMDA) receptor.^{13,18,23} This receptor is a heterotetrameric ion channel generally formed by the two subunits, NR1 and NR2A-D, and gated by glutamate and glycine.²⁴ The NMDA receptor plays a key role in several diseases in the brain,^{24,25} but development of drugs that directly interact with the NMDA receptor has been difficult.²⁶ Therefore, alternative approaches to modulate the NMDA receptor activity are of great interest; one such approach is perturbation of the PSD-95/NMDA receptor interaction. PSD-95 simultaneously binds the NMDA receptor, primarily NR2A and NR2B subunits,^{13,18,23} and the enzyme neuronal nitric oxide synthase

* To whom correspondence should be addressed. Phone: +45 3533 6114. Fax: +45 3533 6040. E-mail: krst@farma.ku.dk.

[†] University of Copenhagen.

[‡] Uppsala University.

^a Abbreviations: Abu, 2-aminobutanoic acid; Aib, α -aminoisobutyric; FP, fluorescence polarization; nNOS, neuronal nitric oxide synthase; NO, nitric oxide; NMDA, *N*-methyl-D-aspartate; PDZ, PSD-95, discs large, zonula occludens-1; PPIs, protein–protein interactions; PSD-95, postsynaptic density-95; WT, wild-type.

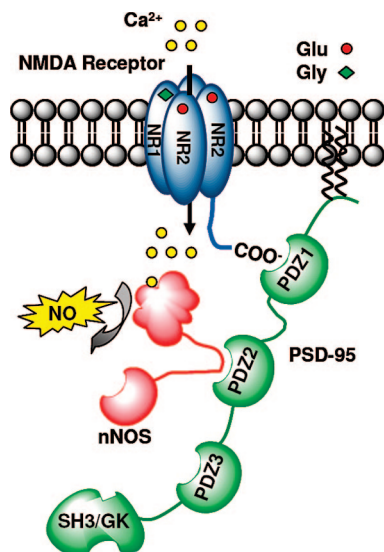


Figure 1. During ischemia an excessive amount of glutamate is released. This release activates the membrane bound NMDA receptors leading to Ca^{2+} ions entering the cells. Because of the colocalization of NMDA receptors and nNOS mediated by PSD-95, this Ca^{2+} influx is coupled to the potential harmful production of NO.

(nNOS) through PDZ1 or PDZ2 (Figure 1). Activation of the NMDA receptor causes influx of Ca^{2+} , which activates nNOS, thereby leading to nitric oxide (NO) generation.^{27,28} Thus, PSD-95 mediates a specific association between NMDA receptor activation and NO production, which can be detrimental for the cells if sustained for a longer period (Figure 1).

It has been shown that inhibition of the PSD-95/NMDA receptor interaction prevents ischemic brain damage in rats, presumably by impairing the functional link between Ca^{2+} entry and NO production, while the physiological function of the NMDA receptor remains intact.²⁹ Uncoupling of PSD-95 from the NR2B subunit was achieved by a nonapeptide, corresponding to the C-terminal of NR2B, fused to HIV-1 Tat peptide, known for its ability to facilitate membrane permeability. This 20-mer peptide is currently in clinical trials as a potential drug for the treatment of cerebrovascular ischemia, as seen in stroke.^{30–32} However, peptides are generally not attractive drug candidates due to their poor bioavailability and instability in vivo. Therefore, there is great interest in transforming the NR2B C-terminal peptide into a more druglike compound, which so far has not been achieved.

To develop a nonpeptide inhibitor of the PSD-95/NMDA receptor interaction, a peptidomimetic approach is attractive because the binding pocket is well-defined and embeds a small, linear peptide motif. However, the binding pocket of PDZ domains has a relatively small surface area and a nonfavorable geometry, which makes PDZ domains difficult to target with small molecules.³³ These difficulties are reflected by the very low number of small molecule inhibitors of PDZ domain interactions.^{34–40} Moreover, the requirement of a deprotonated carboxylic acid do not favor cell permeability or permeability of the blood–brain barrier.⁴¹ In the few cases where reasonable affinities have been achieved, the natural binding peptides have been the starting point for ligand design.^{36,39,40} We have therefore pursued a peptidomimetic strategy in the search for nonpeptide inhibitors of the PSD-95/NMDA receptor interaction using an undecapeptide corresponding to the NR2B C-terminal as a starting point.¹⁸ By a number of modifications used for converting peptides into simplified nonpeptide structures, we have identified small peptide derivatives that demonstrate

Table 1. Validation of FP Assay: K_d and K_i Values of WT Probes and Peptides^a

compound	PDZ1	PDZ2	PDZ3	PDZ1–2
5-FAM/Cy5–NR2B ^b	20 ± 1.6	3.0 ± 0.16	NA ^d	1.7 ± 0.11
5-FAM/Cy5–CRIPT ^b	ND ^d	ND ^d	3.5 ± 0.18	ND ^d
NR2B (1) ^c	18 ± 0.92	4.1 ± 0.17	NA ^d	7.0 ± 0.19
CRIPT (2) ^c	97 ± 18	25 ± 1.6	2.1 ± 0.15	45 ± 4.1
Tat–NR2B (3) ^c	14 ± 1.9	4.4 ± 0.32	NA ^d	9.8 ± 0.35

^a K_d and K_i values are shown as mean ± SEM (standard error of mean) in μM based on at least four individual measurements. ^b K_d values. ^c K_i values. ^d ND: not determined, NA: no affinity.

several-fold improved affinities toward the PDZ domains of PSD-95, thus providing the first steps toward druglike inhibitors of the PSD-95/NMDA receptor interaction.

Results

Validation of the Fluorescence Polarization Assay. A convenient and reliable way to examine interactions between peptide analogues and PDZ domains is by using a fluorescence polarization (FP) assay as has been applied previously in similar studies.^{17,18,42} In this study, we expressed the three PDZ domains, PDZ1–3, of PSD-95 individually, as well as a tandem construct, PDZ1–2. Fluorescent peptides were synthesized by labeling the undecapeptide peptides corresponding to the wild-type (WT) C-terminal of the NR2B subunit (YEKLSIESDV) and CRIPT (LDTKKNYKQTSV) with either 5-FAM or Cy5 (see Supporting Information for chemical structures) through a tripeptide (KSG or CSG) linker, at the N-terminus (designated 5-FAM–NR2B, Cy5–NR2B, 5-FAM–CRIPT, and Cy5–CRIPT).¹⁸ K_d values could then be determined. A competition binding assay was also implemented, which allowed us to measure the affinity as IC_{50} values between PDZ domains and nonfluorescent NR2B (1, KSG–YEKLSIESDV) and CRIPT (2, KSG–LDTKKNYKQTSV) peptides, which were subsequently converted to K_i values.⁴²

Because K_d and K_i values are supposed to be similar when measuring the same PDZ–peptide interaction, these values were compared for the NR2B derived peptides (PDZ1, PDZ2, and PDZ1–2) and CRIPT derived peptides (PDZ3). The K_d and K_i values are very similar when measured against PDZ1, PDZ2, and PDZ3, although the K_i for the tandem construct PDZ1–2 is somewhat higher than K_d (Table 1). Furthermore, the K_d values are independent of whether 5-FAM or Cy5 is used as a fluorophore (data not shown). The K_d for 5-FAM–NR2B peptide was also determined for PDZ2 with and without His-tag, and as expected, no difference was observed (data not shown).^{43,44} Thus, the results obtained in the assay represent accurate measurements, which are confirmed by comparing to literature values for similar measurements.^{17,45,46}

Peptide 1 shows no binding to PDZ3 (Table 1), which is expected,^{18,47} hence affinity at PDZ3 is used as a measure of selectivity throughout this study. All compounds were tested for PDZ3 binding and unless otherwise stated, compounds had no affinity toward this domain.

Finally, we examined the effect of the 20-mer Tat–NR2B peptide (3, YGRKKRRQRRR–KLSSIESDV), which was recently reported to have >100-fold increased affinity to PDZ2 compared to the NR2B peptide alone, as shown by a solid-phase ELISA based assay.³¹ However, in our FP assay, K_i values for PSD-95 PDZ domains are similar for 1 and 3 (Table 1). Thus, the notable in vivo effects demonstrated for this Tat–NR2B peptide²⁹ are more likely due to the ability of the Tat-moiety to improve membrane permeability of peptides rather than increasing the affinity between peptide ligand and the PDZ domains of PSD-95.

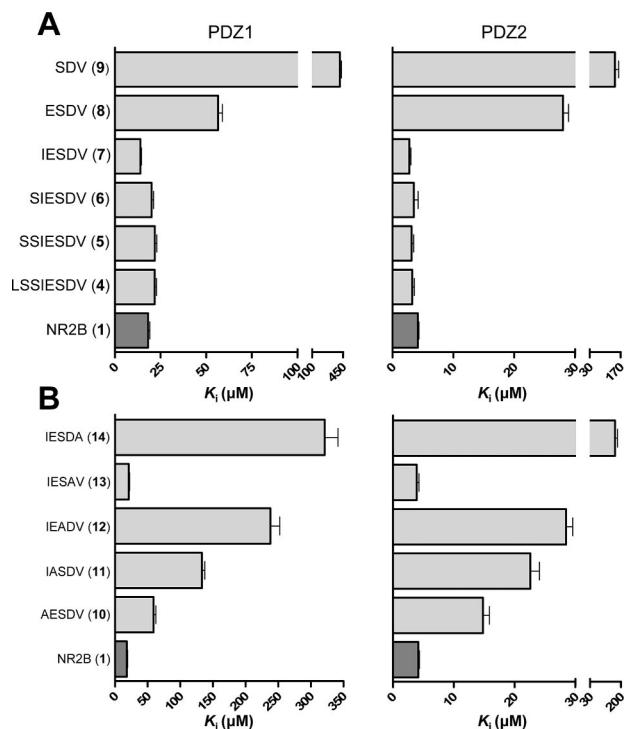
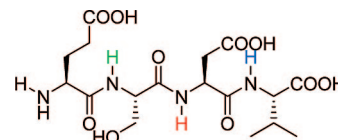


Figure 2. (A) K_i values of truncated peptides for the interaction with PDZ1 and PDZ2. (B) K_i values of Ala-scan performed with pentapeptide **7** toward PDZ1 and PDZ2. Error bars indicate SEM based on at least four individual measurements.

Truncations and Alanine Scan. Initially, the minimal sequence of **1** that was still able to bind PDZ1 and PDZ2 in the FP assay was identified. The peptide was truncated sequentially from the *N*-terminus, and notably it was possible to reduce it to a pentapeptide, IESDV (**7**), without losing affinity (Figure 2A). Truncation to the tetrapeptide ESDV (**8**) showed 3.1- and 6.8-fold increase in K_i values for PDZ1 and PDZ2, respectively, and the tripeptide, SDV, demonstrated >20- and >30-fold increase in K_i compared to peptide **1**. To examine the generality of this approach to PDZ domain proteins, the affinity of peptide **2** at PDZ3 was compared with a truncated CRIPT pentapeptide (KQTSV); in contrast to **1** and PDZ1 and PDZ2, a 14-fold loss in K_i was observed for this pentapeptide (data not shown). This result is in accordance with a previous study, where it was also demonstrated that a CRIPT hexapeptide has similar affinity to **2**.⁴⁵

To investigate the individual importance of the five amino acids in the pentapeptide (**7**), an alanine scan was performed on this peptide (Figure 2B). For both PDZ1 and PDZ2, almost complete loss of affinity was observed when substituting Val in the P⁰ position (**14**), thereby underlining the crucial importance of the isopropyl side chain. A similar effect was observed for PDZ1 when exchanging Ser (P⁻²) (**12**), while a 7-fold increase in the K_i value was seen for PDZ2. Thus positions P⁰ and P⁻² are particularly critical for affinity in the pentapeptide, as has previously been demonstrated for **1**.¹⁸ Two other positions, Glu (P⁻³) and Ile (P⁻⁴), displayed less sensitivity to Ala substitutions (**10** and **11**, respectively), but K_i values were still somewhat higher than **1** toward PDZ1 and PDZ2. On the other hand, replacing Asp (P⁻¹) (**13**) did not affect affinity to PDZ1 or PDZ2, however some affinity at PDZ3 appeared. Although the affinity of **13** toward PDZ3 is low (K_i > 30-fold higher than **2**), this suggests that Asp (P⁻¹) plays a role in determining selectivity between the PDZ domains of PSD-95.

Table 2. K_i Values of *N*-Methylated ESDV Analogues^a



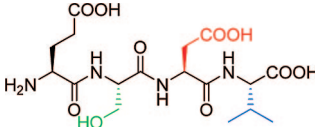
Compound	Position of modification	Structure of modification	PDZ1	PDZ2
NR2B (1)	-	-	18 ± 0.92	4.1 ± 0.17
ESDV (8)	-	-	56 ± 2.4	28 ± 0.92
15	P ⁰	CH ₃	NA ^b	NA ^b
16	P ⁻¹	CH ₃	87 ± 3.1	78 ± 4.5
17	P ⁻²	CH ₃	NA ^b	NA ^b
18	P ⁻³	CH ₃	24 ± 1.8	15 ± 1.2

^a K_i values are shown as mean ± SEM in μ M based on at least four individual measurements. ^b NA: no affinity.

Single Modifications. After having identified the significance of each amino acid by alanine scan of the pentapeptide, we wanted to introduce substitutions that improved affinity and at the same time reduced polarity. We therefore used the tetrapeptide ESDV (**8**) as a template rather than the pentapeptide, because it is a better starting point for development of small molecules and it is still relatively potent at both PDZ1 and PDZ2. Introduction of *D*- and *N*-methyl amino acids can often induce resistance to enzymatic cleavage. Moreover, *D*-amino acids provide information on the importance of stereochemical arrangement of the side chains of the amino acids, while *N*-methyl amino acids are known to stabilize certain amide bond conformations.⁴⁸

Introduction of *D*-Ser, *D*-Asp, and *D*-Val instead of their respective *L*-amino acids one at a time into **8** abolished affinity to both PDZ1 and PDZ2, whereas *D*-Glu impaired the affinity > 25 times for PDZ1 and PDZ2 relative to peptide **1** (data not shown). Thus, *L*-amino acids are essential for affinity. Substitution with *N*-methyl amino acids was better tolerated (Table 2). *N*-methylation of Asp in P⁻¹ (**16**) showed some loss in affinity compared to **8** for both PDZ1 and PDZ2 (Table 2), whereas, *N*-methylation of Val (P⁰) (**15**) and Ser (P⁻²) (**17**) resulted in inactive peptides. However, substituting the terminal amino acid Glu (P⁻³) with *N*-methylated Glu (**18**) improved the affinity relative to the reference tetrapeptide (**8**) and, compared to **1**, **18** showed only 1.3- and 3.7-fold higher K_i values for PDZ1 and PDZ2, respectively (Table 2).

The effects of modifying side chains in **8** were investigated by substituting with proteinogenic and nonproteinogenic amino acids (Table 3) with focus on changes in size and/or polarity in an attempt to optimize PDZ binding and druglikeness. Initially, Val (P⁰) was substituted with relatively conservative unnatural amino acid analogues, as substitutions with Ile, Leu, and Phe have previously been shown to severely impair binding between **1** and PDZ1 and PDZ2.¹⁸ Replacing with either 2-aminobutanoic acid (Abu) or α -aminoisobutyric acid (Aib) to give **19** and **20**, respectively, reduced affinity dramatically (Table 3). Interestingly, when substituting with *tert*-leucine (*t*Leu) (**21**), affinity to PDZ1 was reduced only 4.2-fold, whereas affinity to PDZ2 was reduced ~40-fold relative to **1** (Table 3). This is noteworthy

Table 3. K_i Values of Single Modifications of Tetrapeptide, ESDV^a


Compound	Position of modification	Structure of modification	PDZ1	PDZ2
NR2B (1)	-	-	18 ± 0.92	4.1 ± 0.17
ESDV (8)	-	-	56 ± 2.4	28 ± 0.92
19		CH ₂ CH ₃	230 ± 7.8	NA ^b
20	P ⁰	(CH ₃) ₂	NA ^b	NA ^b
21		C(CH ₃) ₃	76 ± 3.2	160 ± 5.0
22		(CH ₂) ₂ CONH ₂	57 ± 2.3	29 ± 4.1
23	P ⁻¹	(CH ₂) ₂ COOH	67 ± 3.6	29 ± 2.1
24		CH ₂ CONH ₂	88 ± 5.4	67 ± 7.1
25		(CH ₂) ₂ OH	NA ^b	NA ^b
26	P ⁻²	CH(CH ₃)CH ₂ OH	NA ^b	NA ^b
27		C(CH ₃) ₂ CH ₂ OH	NA ^b	NA ^b
28		CH(CH ₃)OH	22 ± 0.95	16 ± 0.85
29	P ⁻³	(CH ₂) ₂ CONH ₂	130 ± 11	100 ± 7.1

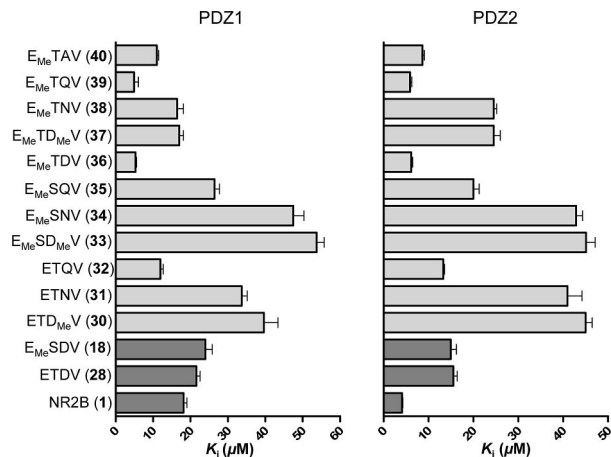
^a K_i values are shown as mean ± SEM in μM based on at least four individual measurements. ^b NA: no affinity.

because it could provide a strategy for designing inhibitors that differentiate affinity at PDZ1 and PDZ2, which is unprecedented.

In the P⁻¹ position, Asp was substituted with Gln, Glu, and Asn (22–24), and extending the acid side chain with one methylene group, as in Glu (23), did not reduce affinity significantly, but amidation of the acid, as in Asn (24), reduced affinity for PDZ1 and PDZ2. However, a combination of the two modifications, substituting Asp with the uncharged Gln (22), did not affect the affinity to either PDZ1 or PDZ2, thus peptide 22 has an affinity similar to 8 (Table 3).

Substitution of Ser (P⁻²) with the nonproteinogenic amino acids homoserine, allo-threonine, and hydroxy-valine, compounds 25–27, led to inactive peptides (Table 3), but substitution with Thr (28) increased the affinity compared to lead peptide 8 and showed only 1.2- and 4-fold increased K_i values compared to 1 for PDZ1 and PDZ2, respectively. A similar increase in affinity has previously been demonstrated for the same substitution in 1.¹⁸ Substituting Glu (P⁻³) with Asp or Asn has previously been shown to reduce affinity dramatically in peptide 1.¹⁸ Here, Glu was substituted with Gln (29), which resulted in impairment of binding (Table 3), and no further substitutions was attempted.

Combination of Substitutions. The studies so far have showed that Thr (28) and *N*-methyl Glu (E_{Me}) (18) in positions P⁻² and P⁻³, respectively, of the tetrapeptide 8 are favorable. Modifications in position P⁰ are generally not allowed, whereas a greater degree of freedom is seen in position P⁻¹. On the basis of these observations, three series of compounds were designed and synthesized: two series of compounds, ETXV and E_{Me}SXV,

**Figure 3.** K_i values of tetrapeptides toward PDZ1 and PDZ2, where individually favorable substitutions have been combined. Error bars indicate SEM based on at least four individual measurements.

with X being Gln, Asn, or *N*-Me-Asp, and a series of compounds, E_{Me}TXV, where X is Gln, Asn, *N*-Me-Asp, Ala, or Asp.

A combination of the two favorable modifications, E_{Me} at P⁻³ and Thr at P⁻², led to compounds with K_i values significantly lower than 1 at PDZ1 and only slightly higher at PDZ2 (Figure 3). Interestingly, the modified tetrapeptides, E_{Me}TDV (36) and E_{Me}TQV (39), are ca. 3-fold more potent than 1 at PDZ1 and only slightly less potent at PDZ2. Introducing the small, nonpolar amino acid Ala in P⁻¹ giving E_{Me}TAV (40) provided an inhibitor that was more potent than 1 at PDZ1 and only 2-fold less potent for PDZ2. Although 40 demonstrated some affinity at PDZ3, the K_i value at PDZ3 was still considerably higher (~79 μM) relative to that of PDZ1 and PDZ2, thus 40 is considered selective toward PDZ1 and PDZ2 relative to PDZ3. Substituting in the P⁻¹ position with *N*-Me-Asp (37) or Asn (38) reduced affinity compared to 36, but these peptides were still equally potent toward PDZ1 compared to peptide 1 (Figure 3).

Tripeptides and *N*-Terminal Acetylation. Encouraged by the studies of tetrapeptides, two series of tripeptides were designed and synthesized: TXV and T_{Me}XV peptides, where X was Asp, Gln, Asn, or *N*-Me-Asp and, additionally, Gly and Ala were incorporated in the TXV structure. TAV (49) and TDV (41) were the most potent tripeptides with K_i values only ~2- and 10-fold higher than 1 at PDZ1 and PDZ2, respectively (Figure 4). Thus, 49 and 41 are surprisingly effective in binding to particularly PDZ1, considering their dramatic truncation from the NR2B peptide. For all other substitutions in the P⁻¹ position, there was a greater loss in affinity, and in the tripeptide series, *N*-methylation did not improve affinity as seen for the tetrapeptides (Figure 4). In terms of peptidomimetic design, Ala would simplify synthesis of future nonpeptide analogues, thus 49 is preferred as a template for further studies. In an attempt to simplify the structure even further, replacing with Gly to give TGV (50) was examined but resulted in severe loss of affinity at both PDZ1 and PDZ2.

To probe the importance of the *N*-terminal amino group in the tetra- and tripeptides, the primary amino group was acetylated. There was a clear difference in effect; there was no effect on affinity toward either PDZ domains upon acetylation of tetrapeptide 51, whereas acetylation of tripeptide 49 significantly impaired the affinity (data not shown). Finally, the amino group of 49 was replaced with hydrogen by substitution of Thr with (*R*)-3-hydroxybutanoic acid, leading to modified tripeptide with

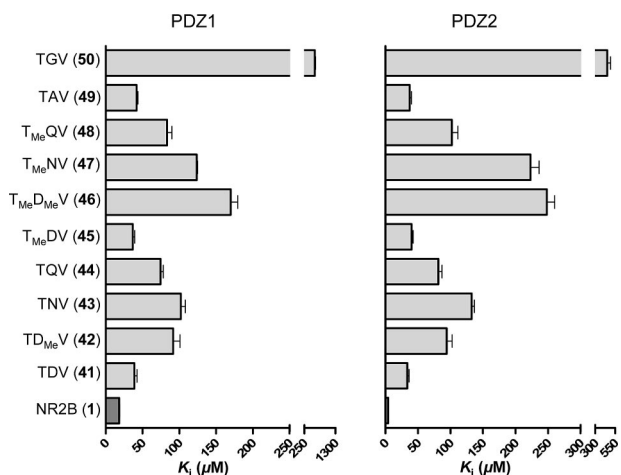


Figure 4. K_i values of tripeptides with one or two substitutions toward the interaction with PDZ1 and PDZ2. Error bars indicate SEM based on at least four individual measurements.

severe impairment in affinity (>100 -fold change for PDZ1 and PDZ2, data not shown).

Throughout this study, the compounds were evaluated in a FP assay. It is well-established that one of the primary issues in the search for new ligands for PPIs is the occurrence of false positives. Therefore, the activities of relevant compounds were validated in a secondary assay. Thus, the relative affinities for compound **1**, **3**, **7–9**, **40**, and **49** were determined in a pull-down assay and the data confirmed the results from the FP assay (see Supporting Information).

Molecular Modeling and Docking. Homology models of PDZ1 and PDZ2 were generated using Prime based on the X-ray crystallographic structure of PDZ3 in complex with CRIPT peptide,²⁰ and flexible docking of key peptides was performed using Glide. Initially, the pentapeptide **7** was docked into PDZ1, resulting in a binding mode where the backbone of **7** superimposed with the backbone of the CRIPT peptide in PDZ3. However, an electrostatic interaction not found in the PDZ3–CRIPT

structure emerged between the *N*-terminal amino group of **7** and Asp90 in the large β B– β C loop of PDZ1 (Figure 5A). A hydrophobic pocket was formed by Thr 83, Gly89, and His130 in PDZ1 (PDZ2: His225, Val178, and Pro184), which was partially filled by the side chain of Ile in position P^{-4} . The Glu residue in P^{-3} interacted with Thr97 and Lys98 from the β C strand of PDZ1 (PDZ2: Thr192 and Lys193) through hydrogen bonding and electrostatic forces, explaining the importance of this residue for affinity (Figure 5A). The hydroxyl group of Ser in P^{-2} formed a hydrogen bond with His130, similar to that observed in the PDZ3–CRIPT structure. Replacing Ser (P^{-2}) with Thr allows the additional methyl group to interact with a hydrophobic area created by Val134 in PDZ1 (PDZ2: Val229) as previously demonstrated,¹⁸ this may explain the increased affinity upon the Ser-to-Thr substitution. Substitutions with larger unnatural amino acids in P^{-2} are probably not allowed due to steric clashes with the PDZ residues.

In the PDZ3–CRIPT structure, the side chain of P^{-1} does not interact with a residue in PDZ3.²⁰ In our model, we see an electrostatic interaction between Asp (P^{-1}) and Lys98 (Figure 5A), in accordance with previous results.¹⁸ Structural studies of other PDZ domains have demonstrated a salt bridge between the amino acid in P^{-1} and PDZ domains,⁴⁹ which has also been indicated by functional studies.¹⁵ We observed that Asp could be replaced with Gln or Ala, indicating that neither charge nor hydrogen bonding is crucial for affinity. On the other hand, introduction of Asn in the P^{-1} position reduced the affinity more extensively, demonstrating that not all side chain substitutions are equally allowed.

We observed that methylation of the *N*-terminal amino group enhanced the affinities for the tetrapeptides but not for tripeptides. Docking of *N*-methylated tetrapeptide **40** into PDZ1 reveals that the *N*-terminal amino group is in close proximity to His130, thereby creating a favorable cation– π interaction (Figure 5B). The interaction is further stabilized by the *N*-methyl group, which is situated in the π -system of the imidazole ring of His130 (Figure 5B), which explains the increased affinity upon *N*-methylation. Side chain groups of positions P^0 , P^{-2} ,

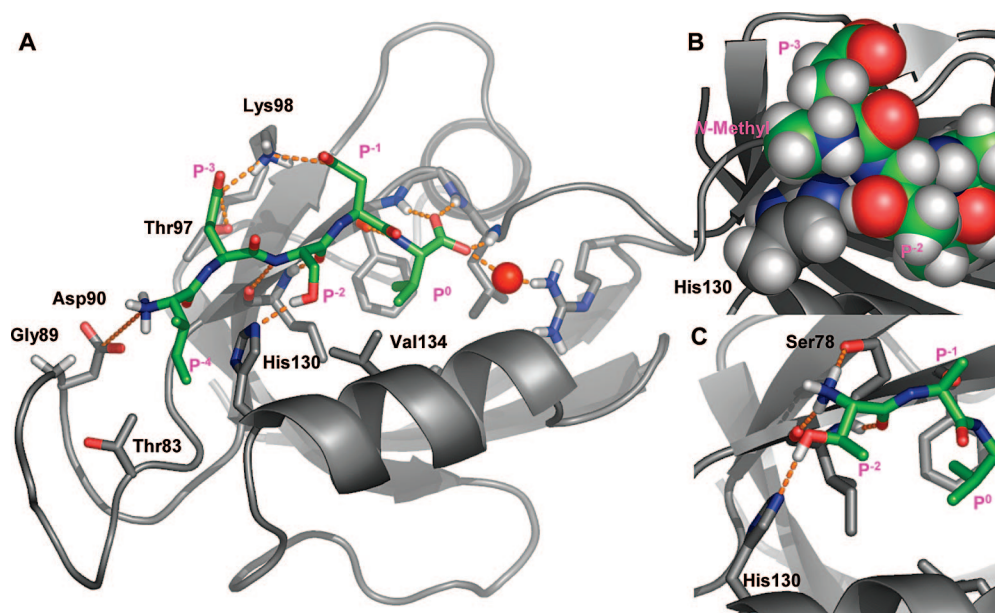
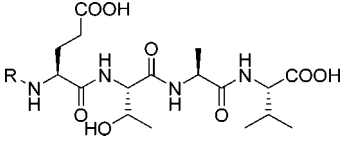
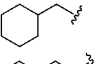
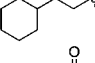
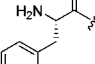
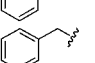
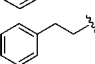
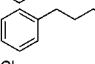
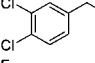
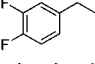
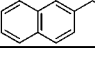


Figure 5. Peptides docked into the PDZ1 homology model. (A) **7**; (B) **40**; (C) **49**. Ligands are shown using green carbons; selected side chains from PDZ are shown with gray carbons; nitrogens are blue, oxygens are red and key hydrogen atoms are shown in white; the coordinated water is depicted as a red sphere; hydrogen bonds and electrostatic interactions are indicated with orange dashes. PDZ residues mentioned in the text are labeled in black, and ligand side chain positions are shown in magenta.

Table 4. K_i Values of *N*-Terminally Modified ETAV Peptides^a


Compound	R	PDZ1	PDZ2	PDZ3
NR2B (1)	-	18 ± 0.92	4.1 ± 0.17	NA ^b
CRIP1 (2)	-	97 ± 18	25 ± 1.6	2.1 ± 0.15
ETAV (51)	-	29 ± 1.6	22 ± 0.92	260 ± 20
40	CH ₃	11 ± 0.47	8.9 ± 0.50	78 ± 1.5
52	CH ₂ CH ₃	9.3 ± 0.55	9.6 ± 0.80	69 ± 2.8
53	(CH ₂) ₂ CH ₃	7.0 ± 0.28	4.2 ± 0.20	35 ± 1.0
54	(CH ₂) ₃ CH ₃	8.4 ± 0.37	4.0 ± 0.36	35 ± 0.82
55		1.0 ± 0.24	1.3 ± 0.094	21 ± 0.64
56		0.94 ± 0.13	0.45 ± 0.13	11 ± 0.43
57		6.3 ± 0.38	2.3 ± 0.27	35 ± 1.3
58		7.2 ± 0.39	5.2 ± 0.22	63 ± 2.4
59		4.4 ± 0.49	1.6 ± 0.19	14 ± 0.54
60		2.1 ± 0.35	3.1 ± 0.31	44 ± 2.5
61		2.4 ± 0.25	1.1 ± 0.11	6.7 ± 0.20
62		0.98 ± 0.06	1.0 ± 0.043	7.8 ± 0.34
63		1.0 ± 0.33	0.95 ± 0.05	10 ± 0.22

^a K_i values are shown as mean ± SEM in μ M based on at least four individual measurements. ^b NA: no affinity.

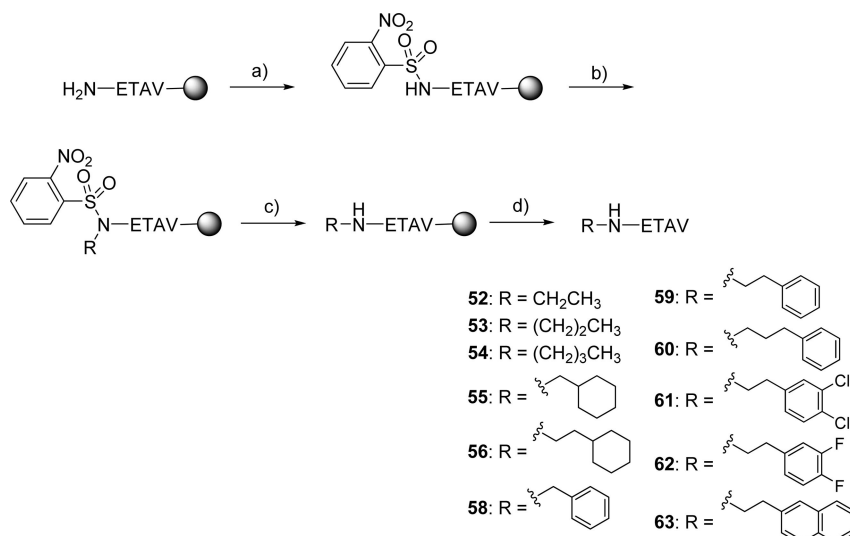
and P⁻³ and ligand backbone are bound to PDZ in the same configuration as for the pentapeptide **7**. Docking of tripeptide **49** into the PDZ1 homology model show that the *N*-terminal amino group mediates charge assisted hydrogen bonding to the hydroxyl oxygen of Ser78 (PDZ2: Ser173) and a backbone carbonyl group (Figure 5C). This binding motif correlates with the observation that *N*-methylation of tripeptides did not improve affinity because no additional interactions were obtained.

***N*-Terminal Modifications of ETAV.** The molecular modeling studies suggested that the methyl group in **40** only partially overlaps with the His130 aromatic side chain in PDZ1 (Figure 5B). We therefore hypothesized that replacing the methyl group with larger groups could improve affinity through increased hydrophobic interactions and/or aromatic stacking interactions. A series of ETAV (**51**) analogues were therefore designed and synthesized where the *N*-terminal amino group was alkylated with larger aliphatic and aromatic substituents (Table 4). *N*-alkylation of ETAV was facilitated by a Mitsunobu reaction using the Fukuyama protocol,⁵⁰ as previously applied for preparation of *N*-alkylated peptides.⁵¹ The terminal amino group of ETAV was activated as a nitrobenzyl sulfonamide and

subsequently reacted with a range of alcohols mediated by diisopropyl azodicarboxylate (DIAD) and Ph₃P to give the protected, resin-bound products (Scheme 1). The final products were obtained by deprotection of the sulfonamide and cleavage from the resin, providing the desired products, compounds **52–56** and **58–63**, in excellent purity and generally great yield (Table 4).

Initially, the methyl group of **40** was replaced with ethyl (**52**), propyl (**53**), and butyl (**54**); molecular docking studies specifically suggested that ethylated ETAV (**52**) would have similar affinity to E_{Me}TAV (**40**), whereas propylated and butylated ETAV (**53** and **54**) should have increased affinity. Biological evaluation of the compounds confirmed this prediction, particularly for affinity at PDZ2 (Table 4). Generally, the increased affinity was more pronounced for PDZ2 than PDZ1, and compounds **53** and **54** were equipotent to **1** at PDZ2 and ca. 2-fold more potent at PDZ1. In addition affinity toward PDZ3 was also increased, although a significant selectivity for PDZ1 and PDZ2 remain (Table 4). Increasing the bulk and hydrophobicity of the *N*-alkyl substituents even further, modifying ETAV with cyclohexylmethyl (**55**) and cyclohexylethyl (**56**), led to dramatic increases in affinity. Compared to the starting point (**1**), compounds **55** and **56** shows a ca. 19-fold increase in affinity toward PDZ1 and **56** shows a 9-fold increase in affinity toward PDZ2. Thus, peptide derivative **56** is a very potent inhibitor of the PSD-95/NMDA receptor interaction and to the best of our knowledge is the most potent compound reported to date.

Encouraged by this improvement of affinity, we turned our attention to substitutions with an aromatic group, which our modeling studies had suggested would also improve affinities compared to **40** and **51–54**. Initially, we prepared the pentapeptide, FETAV (**57**), with an aromatic side chain in the P⁻⁴ position. The pentapeptide **57** had a 3- and 2-fold increase in affinity at PDZ1 and PDZ2, respectively, compared to **1**, thus confirming that an aromatic substituents in P⁻⁴ is favorable. This prompted the synthesis of peptide derivatives, where the *N*-terminus of ETAV was alkylated with aromatic substituents as in compounds **58–63** (Table 4). All of the six peptide derivatives (**58–63**) had improved affinity compared to both **1** and **40**. The length of the spacer between the aromatic group and the terminal amino group is important, and a gradual increase in affinity for PDZ1 is seen when extending from methylene (**58**), ethylene (**59**) to propylene spacer (**60**), whereas the ethylene spacer (**59**) is the most potent at PDZ2 (Table 4). Next, the effect of substituting the aromatic ring was investigated; substitution with two chlorine atoms (**61**) increased affinity compared to **59** at both PDZ1 and PDZ2. Replacing chlorine with fluorine (**62**) increased affinity even further, and **62** showed K_i values around 1 μ M at both PDZ1 and PDZ2, thus being almost equipotent to the cyclohexylethyl derivative **56**. Thus changing the electronic properties of the aromatic ring affects affinity, which is suggested by modeling studies to be due to the interaction of the aromatic group with His130 of PDZ1. Docking compounds **59** and **61–62** into the homology model of PDZ1 suggest a perpendicular stacking between the aromatic group from the peptides and His130. Increasing the bulk of the aromatic group further to a naphthalene-2-yl moiety (**63**) resulted in a compound equipotent to **62**. For all compounds, a considerable increase in affinity toward PDZ3 was observed. However, a significant selectivity is preserved and

Scheme 1^a

^a Reagents and conditions: (a) *o*-Nitrobenzenesulfonyl chloride, DIPEA. (b) Ph₃P, ROH, DIAD (c) NaSPh, DMF (d) TFA, TIPS, H₂O (90:5:5).

for the most potent inhibitor, **56**, a 10- and 20-fold selectivity toward PDZ1 and PDZ2 relatively to PDZ3 is seen (Table 3).

Conclusion

In this study, we have exploited the NR2B undecapeptide **1** as a template for development of smaller molecules with the potential of uncoupling the PPI between PSD-95 and the NMDA receptor. A peptidomimetic approach was followed, starting with truncation of **1** from its *N*-terminus to a pentapeptide **7**, without loss of affinity toward PDZ1 and PDZ2 of PSD-95, whereas further deletion reduced affinity. The decrease in affinity could be compensated by substituting Glu and Ser of the tetrapeptide ESDV with *N*-Me-Glu and Thr, respectively, thereby resulting in *N*-methylated tetrapeptide, **36**, with improved affinity to PDZ1 and essentially WT affinity at PDZ2. The Asp residue could be replaced with the noncharged Gln or the hydrophobic Ala without affecting affinity significantly, providing **40** as a promising lead. Interestingly, the tripeptide **49** is still a reasonably potent inhibitor of PDZ1 and PDZ2, with *K*_i values of 42 and 37 μM, respectively, thus only ca. 2- and 9-fold less potent than **1**, while still showing selectivity within the PDZ domains of PSD-95.

Guided by molecular modeling and docking of peptides and modified peptides into a homology model of PDZ1, modification of the *N*-terminal methyl group of **40** was pursued. Applying the Fukuyama protocol of the Mitsunobu reaction allowed the preparation of 11 *N*-alkylated tetrapeptides, which all had superior affinity at PDZ1 and PDZ2 compared to the lead peptide **40**. In particular, replacing the methyl group with cyclohexylethyl, compound **56** provided the most potent inhibitor of the PSD-95/NMDA receptor interaction, with *K*_i values of 0.94 and 0.45 μM at PDZ1 and PDZ2, respectively. In addition, introduction of aromatic substituents provided almost equipotent compounds, with **62** and **63** being the most potent. Although, PDZ3 binding was also increased by the *N*-terminal alkylations, a considerable selectivity toward PDZ1 and 2 was still observed. Further studies will elucidate the selectivity for a wider range of PDZ domains.

Thus, *N*-terminal modifications and optimization of side chains in a tetrapeptide have hereby provided the most potent inhibitor of the PSD-95/NMDA receptor interaction, with a ca. 20-fold increase in affinity compared to the WT peptide. Besides having improved potency, compound **56** shows a reduction in

number of charges and overall polarity compared to **1**. Thus, both the modified tetrapeptides and the tripeptide are very promising leads for further optimizations toward even more druglike compounds. In addition, considering the close structural similarity between PDZ domains with respect to sequence homology and ligand recognition, the strategy presented here could be applicable for other PDZ domains with potential interest in drug development.

Experimental Section

Chemistry. Proton (¹H) NMR spectra were recorded on Bruker spectrometers: Avance 300 NMR (300 MHz). Chemical shifts (δ) are reported in parts per million (ppm) with reference to tetramethylsilane (TMS) as internal standard. NMR experiments were carried out in CD₃OD. The following abbreviations are used for the proton spectra multiplicities: s, singlet; d, doublet; dd, double doublet, triplet; q, quartet; m, multiplet. Coupling constants (*J*) are reported in Hertz (Hz). Mass spectra were obtained with an Agilent 6410 triple quadrupole mass spectrometer instrument using electron spray coupled to an Agilent 1200 HPLC system (ESI-LC/MS) with autosampler and diode-array detector using a linear gradient of the binary solvent system of water/acetonitrile/TFA (A: 95/5/0.1; B: 5/95/0.086) with a flow rate of 1 mL/min. During ESI-LC/MS analysis, evaporative light scattering (ELS) traces were obtained with a Sedere Sedex 85 light scattering detector, which were used for estimation of the purity of the final products. High resolution mass spectra (HRMS) were obtained using a Micromass Q-ToF 2 instrument and were all within ±5 ppm of theoretical values. Preparative HPLC was performed on a Agilent 1100 system using a C18 reverse phase column (Zorbax 300 SB-C18, 21.2 mm × 250 mm) with a linear gradient of the binary solvent system of water/acetonitrile/TFA (A: 95/5/0.1; B: 5/95/0.086) with a flow rate of 20 mL/min and UV detection at 230 nm.

Peptide Synthesis. Peptides were manually synthesized by Fmoc-based solid-phase peptide synthesis (SPPS) using a MiniBlock (Mettler-Toledo, Columbus, OH). Peptides with *C*-terminal Val or Ala were synthesized from preloaded Wang resins (Novabiochem, Darmstadt, Germany). For peptides with an unnatural amino acid in the *C*-terminal, a 2-chloro-trityl resin was used and the first amino acid was loaded on the resin using diisopropylethylamine (DIPEA) (resin/amino acid/DIPEA in 1:4:8) in DCM for 30 min, followed by capping with methanol (DCM/MeOH/DIPEA 17:2:1). Fmoc deprotection was performed with 20% piperidine in DMF (2 × 10 min), and coupling of the consecutive amino acid was carried out with *O*-(benzotriazol-1-yl)-*N,N,N',N'*-tetramethyluronium hexafluorophosphate (HBTU) and DIPEA (resin/amino acid/HBTU/DIPEA

1:4:4:4) and monitored by the ninhydrin test. The final peptide was cleaved from the resin by treatment with 5% water and 5% triisopropylsilane (TIPS) in trifluoroacetic acid (TFA) for 2 h. The crude peptide was purified by preparative HPLC to >98% purity. The peptide was analyzed by ESI-LC/MS and lyophilized. Quantification of peptides was done by weighing. Key peptides (5-FAM-NR2B, 1 and 3) were analyzed by amino acid analysis (Alphalyse, Odense, Denmark) and the molar extinction coefficients were thereby determined. The 5-FAM (Anaspec, San Jose, CA) was attached to the peptides by coupling with *O*-(7-azabenzotriazol-1-yl)-*N,N,N',N'*-tetramethyluronium hexafluorophosphate (HATU). Similarly, *N*-methylated amino acids and the amino acid following the *N*-methylated amino acid were coupled to the growing peptide using HATU. Cy5 conjugated NR2B (Cy5-NR2B) was synthesized by coupling Cy5-maleimide (GE Healthcare, UK) to the cysteine side chain of the peptide sequence CSG-YEKLSSIESDV in solution followed by HPLC purification and ESI-LC/MS analysis. The reaction was performed in a 1:1 ratio between peptide and Cy5-maleimide in 1 × TBS buffer for 2 h at room temperature. Quantification of Cy5-peptides was achieved by measuring absorbance using the molar extinction coefficient of Cy5. Two fluorescent PDZ3 binding peptides, based on the CRIPT sequence (KSG/CSG-LDTKNYKQTSV),⁴⁷ were synthesized with 5-FAM and Cy5, respectively, as described above for NR2B. *N*-Terminal acetylated peptides were synthesized by treating the deprotected peptide with acetic anhydride in DIPEA and DMF (1:2:3) for 1 h, followed by TFA cleavage, purification, and characterization as described above.

***N*-Terminal Alkylation of Peptides. General Procedure.** Peptide (0.25 mmol, 1 equiv) was synthesized on a 2-chloro-trityl resin as described above followed by Fmoc-deprotection, washing, and drying of the resin. The resin was swelled in DIPEA (6 equiv) in THF (2.5 mL) and 2-nitrobenzenesulfonyl chloride (4 equiv) in CH₂Cl₂ (1 mL) was added slowly while agitating the solution. After shaking at room temperature for 3 h, the resin was drained and washed with THF, MeOH, DCM, and THF (flow washes for 2 min.). Subsequently, the resin was treated with triphenylphosphine (Ph₃P, 2 M in THF, 5 equiv) and the alcohol (ROH, 10 equiv) in dry THF (1.0 mL) under nitrogen. DIAD (1 M in THF, 5 equiv) was introduced slowly, followed by agitation for 1 h at room temperature. The resin was then drained and washed with THF and DCM (flow washes). The resin-bound alkylated sulfonamide was swelled in 2 mL DMF and treated with NaSPh/DMF solution (1 M, 2 mL) for 1 h. This was repeated four times to ascertain full deprotection, after which the resin was washed and the modified peptide cleaved from the resin, purified, and characterized as described previously.

***N*-Methyl-ETAV (40).** Yield: 80%. ESI-LC/MS: >99% (ELSD), 98% (UV). ¹H NMR (CD₃OD) δ (ppm): 4.47 (q, *J* = 7.2, 1H), 4.44 (d, *J* = 4.8, 1H), 4.30 (d, *J* = 5.6, 1H), 4.18–4.14 (m, 1H), 3.97 (dd, *J* = 7.2, 5.6 Hz, 1H), 2.68 (s, 3H), 2.53 (t, *J* = 7.4, 2H), 2.19–2.14 (m, 3H), 1.39 (d, *J* = 7.2, 3H), 1.23 (d, *J* = 6.4, 3H), 0.97 (d, *J* = 6.6, 6H). HRMS (ESI+) calcd for C₁₈H₃₃N₄O₈ [M + H]⁺, 433.2298; found, *m/z* 433.2315.

***N*-Ethyl-ETAV (52).** Yield: 71%. ESI-LC/MS: >99% (ELSD), >99% (UV). ¹H NMR (CD₃OD) δ (ppm): 4.47 (q, *J* = 6.8, 1H), 4.44 (d, *J* = 5.2, 1H), 4.30 (d, *J* = 6.0, 1H), 4.17–4.13 (m, 1H), 4.03 (dd, *J* = 7.6, 5.2 Hz, 1H), 3.06–3.03 (m, 2H), 2.53 (t, *J* = 7.4, 2H), 2.19–2.13 (m, 3H), 1.38 (d, *J* = 7.2, 3H), 1.32 (t, *J* = 7.4, 3H), 1.22 (d, *J* = 6.4, 3H), 0.97 (d, *J* = 6.8, 6H). HRMS (ESI+) calcd for C₁₉H₃₅N₄O₈ [M + Na]⁺, 469.2274; found, *m/z* 469.2280.

***N*-Propyl-ETAV (53).** Yield: 95%. ESI-LC/MS: >99% (ELSD), >99% (UV). ¹H NMR (CD₃OD) δ (ppm): 4.47 (q, *J* = 6.8, 1H), 4.44 (d, *J* = 5.2, 1H), 4.30 (d, *J* = 5.2, 1H), 4.17–4.14 (m, 1H), 4.02 (dd, *J* = 7.6, 5.2 Hz, 1H), 2.98–2.88 (m, 2H), 2.54 (t, *J* = 7.4, 2H), 2.21–2.12 (m, 3H), 1.76–1.70 (m, 2H), 1.38 (d, *J* = 7.2, 3H), 1.22 (d, *J* = 6.4, 3H), 1.0 (t, *J* = 7.4, 3H), 0.97 (d, *J* = 6.8, 6H). HRMS (ESI+) calcd for C₂₀H₃₇N₄O₈ [M + H]⁺, 461.2611; found, *m/z* 461.2624.

***N*-Butyl-ETAV (54).** Yield: 94%. ESI-LC/MS: >99% (ELSD), >99% (UV). ¹H NMR (CD₃OD) δ (ppm): 4.47 (q, *J* = 7.2, 1H),

4.44 (d, *J* = 5.2, 1H), 4.30 (d, *J* = 5.6, 1H), 4.17–4.14 (m, 1H), 4.02 (dd, *J* = 7.2, 5.2 Hz, 1H), 3.00–2.93 (m, 2H), 2.54 (t, *J* = 7.4, 2H), 2.21–2.12 (m, 3H), 1.70–1.65 (m, 2H), 1.45–1.40 (m, 2H), 1.38 (d, *J* = 7.2, 3H), 1.22 (d, *J* = 6.4, 3H), 1.0 (t, *J* = 7.4, 3H), 0.97 (d, *J* = 6.8, 6H). HRMS (ESI+) calcd for C₂₁H₃₉N₄O₈ [M + H]⁺, 475.2768; found, *m/z* 475.2770.

***N*-Cyclohexylmethyl-ETAV (55).** Yield: 8%. ESI-LC/MS: >99% (ELSD), >99% (UV). ¹H NMR (CD₃OD) δ (ppm): 4.45 (q, *J* = 7.2, 1H), 4.41 (d, *J* = 4.8, 1H), 4.28 (d, *J* = 5.4, 1H), 4.17–4.12 (m, 1H), 3.94 (dd, *J* = 7.2, 5.6 Hz, 1H), 2.82 (d, *J* = 6.6, 1H), 2.76 (d, *J* = 7.2, 1H), 2.56 (t, *J* = 7.4, 2H), 2.18–2.12 (m, 3H), 1.86–1.68 (m, 6H), 1.38 (d, *J* = 7.2, 3H), 1.32–1.25 and 1.08–1.01 (m, 5H), 1.22 (d, *J* = 6.0, 3H), 0.96 (d, *J* = 6.6, 6H). HRMS (ESI+) calcd for C₂₄H₄₃N₄O₈ [M + H]⁺, 515.3081; found, *m/z* 515.3091.

***N*-Cyclohexylethyl-ETAV (56).** Yield: 56%. ESI-LC/MS: >99% (ELSD), >99% (UV). ¹H NMR (CD₃OD) δ (ppm): 4.45 (q, *J* = 7.2, 1H), 4.42 (d, *J* = 4.8, 1H), 4.29 (d, *J* = 5.4, 1H), 4.16–4.12 (m, 1H), 3.99 (dd, *J* = 7.2, 5.4 Hz, 1H), 3.03–2.91 (m, 2H), 2.53 (t, *J* = 7.4, 2H), 2.22–2.06 (m, 3H), 1.76–1.66 and 1.32–1.25 (m, 10H), 1.58 (q, *J* = 7.2, 1H), 1.38 (d, *J* = 7.2, 3H), 1.22 (d, *J* = 6.3, 3H), 0.97 (d, *J* = 6.9, 6H). HRMS (ESI+) calcd for C₂₅H₄₅N₄O₈ [M + H]⁺, 529.3237; found, *m/z* 529.3214.

***N*-Benzyl-ETAV (58).** Yield: 66%. ESI-LC/MS: >99% (ELSD), 97% (UV). ¹H NMR (CD₃OD) δ (ppm): 7.49–7.41 (m, 5H), 4.48 (q, *J* = 7.2, 1H), 4.44 (d, *J* = 4.8, 1H), 4.28 (d, *J* = 5.4, 1H), 4.16 (s, 2H), 4.12–4.01 (m, 2H), 2.54 (t, *J* = 6.9, 2H), 2.22–2.11 (m, 3H), 1.38 (d, *J* = 7.2, 3H), 1.24 (d, *J* = 6.3, 3H), 0.97 (d, *J* = 6.6, 6H). HRMS (ESI+) calcd for C₂₄H₃₇N₄O₈ [M + H]⁺, 509.2611; found, *m/z* 509.2595.

***N*-Phenylethyl-ETAV (59).** Yield: 11%. ESI-LC/MS: 98% (ELSD), 98% (UV). ¹H NMR (CD₃OD) δ (ppm): 7.35–7.23 (m, 5H), 4.45 (q, *J* = 6.9, 1H), 4.42 (d, *J* = 4.8, 1H), 4.28 (d, *J* = 5.4, 1H), 4.13–4.09 (m, 1H), 4.05 (dd, *J* = 7.2, 5.1 Hz, 1H), 3.23–3.15 (m, 2H), 3.00 (t, *J* = 7.8, 2H), 2.54 (t, *J* = 7.2, 2H), 2.22–2.12 (m, 3H), 1.38 (d, *J* = 7.2, 3H), 1.20 (d, *J* = 6.3, 3H), 0.96 (d, *J* = 6.9, 6H). HRMS (ESI+) calcd for C₂₅H₃₉N₄O₈ [M + H]⁺, 523.2768; found, *m/z* 523.2787.

***N*-Phenylpropyl-ETAV (60).** Yield: 30%. ESI-LC/MS: 98% (ELSD), 97% (UV). ¹H NMR (CD₃OD) δ (ppm): 7.48 (d, *J* = 8.1, 1H), 7.46 (d, *J* = 1.2, 1H), 7.20 (dd, *J* = 8.4, 2.1, 1H), 4.45 (q, *J* = 6.9, 1H), 4.41 (d, *J* = 5.1, 1H), 4.28 (d, *J* = 5.4, 1H), 4.15–4.09 (m, 1H), 4.05 (dd, *J* = 7.2, 5.4 Hz, 1H), 3.27–3.13 (m, 2H), 2.99 (t, *J* = 7.8, 2H), 2.54 (t, *J* = 7.2, 2H), 2.22–2.09 (m, 3H), 1.38 (d, *J* = 7.5, 3H), 1.21 (d, *J* = 6.6, 3H), 0.96 (d, *J* = 6.6, 6H). HRMS (ESI+) calcd for C₂₆H₄₁N₄O₈ [M + H]⁺, 537.2924; found, *m/z* 537.2928.

***N*-(3,4-Dichlorophenyl)propyl-ETAV (61).** Yield: 20%. ESI-LC/MS: 98% (ELSD), 97% (UV). ¹H NMR (CD₃OD) δ (ppm): 7.26–7.17 (m, 2H), 7.09–7.04 (m, 1H), 4.45 (q, *J* = 6.9, 1H), 4.41 (d, *J* = 5.1, 1H), 4.28 (d, *J* = 5.4, 1H), 4.15–4.09 (m, 1H), 4.05 (dd, *J* = 7.2, 5.4 Hz, 1H), 3.27–3.13 (m, 2H), 2.99 (t, *J* = 7.8, 2H), 2.54 (t, *J* = 7.2, 2H), 2.22–2.09 (m, 3H), 1.38 (d, *J* = 7.5, 3H), 1.21 (d, *J* = 6.6, 3H), 0.96 (d, *J* = 6.6, 6H). HRMS (ESI+) calcd for C₂₅H₃₇Cl₂N₄O₈ [M + H]⁺, 591.1988; found, *m/z* 591.1967.

***N*-(3,4-Difluorophenyl)propyl-ETAV (62).** Yield: 12%. ESI-LC/MS: 98% (ELSD), 98% (UV). ¹H NMR (CD₃OD) δ (ppm): 7.85–7.79 (m, 3H), 7.74–7.72 (m, 1H), 7.47–7.44 (m, 3H), 7.37 (dd, *J* = 8.7, 1.8, 1H), 4.45 (q, *J* = 6.9, 1H), 4.42 (d, *J* = 4.8, 1H), 4.28 (d, *J* = 5.4, 1H), 4.13–4.06 (m, 2H), 3.34–3.14 (m, 4H), 2.545 (t, *J* = 7.5, 2H), 2.21–2.15 (m, 3H), 1.38 (d, *J* = 7.2, 3H), 1.19 (d, *J* = 6.3, 3H), 0.96 (d, *J* = 6.9, 6H). HRMS (ESI+) calcd for C₂₅H₃₇F₂N₄O₈ [M + H]⁺, 559.2579; found, *m/z* 559.2591.

***N*-(Naphthalene-2-yl)ethyl-ETAV (63).** Yield: 49%. ESI-LC/MS: >99% (ELSD), >99% (UV). ¹H NMR (CD₃OD) δ (ppm): 7.29–7.15 (m, 5H), 4.45 (q, *J* = 6.9, 1H), 4.40 (d, *J* = 4.8, 1H), 4.28 (d, *J* = 5.4, 1H), 4.14–4.10 (m, 1H), 3.99 (dd, *J* = 7.2, 5.1 Hz, 1H), 2.96–2.91 (m, 2H), 2.70 (t, *J* = 7.2, 2H), 2.52 (t, *J* = 7.2, 2H), 2.19–2.08 (m, 3H), 2.06–1.98 (m, 2H), 1.38 (d, *J* =

7.2, 3H), 1.17 (d, $J = 6.6$, 3H), 0.96 (d, $J = 6.9$, 6H). HRMS (ESI+) calcd for $C_{29}H_{41}N_4O_8$ $[M + H]^+$, 573.2898; found, m/z 573.2897.

Expression and Purification of PDZ1, PDZ2, PDZ3, and PDZ1–2 of PSD-95. The cDNA coding for PSD-95 PDZ1 (residues 61–151), PDZ2 (residues 155–249), PDZ3 (residues 309–401), and PDZ1–2 (residues 61–249) tandem were amplified by inverted PCR and cloned in modified His-tagged pRSET vector (Invitrogen, Carlsbad, CA) (numbers in parenthesis refer to the residue numbers in the human full-length PSD95 α without exon 4b). All PDZ constructs contained an extra sequence, MHHHH-HPRGs, which was used as a tag for purification (His-tag). Competent *Escherichia coli* bacteria (BL21–DE3, pLysS) were transformed with PDZ expressing constructs and grown overnight on agar plates containing ampicillin (100 μ g/mL) and chloramphenicol (35 μ g/mL) at 37 °C. Colonies were picked and used to inoculate bacterial cultures (LB medium with 50 μ g/mL ampicillin). These were stirred while being incubated at 37 °C until A_{600} reached 0.95 for PDZ1, PDZ2, and PDZ3 or 0.45 for PDZ1–2, at which point 1 mM isopropyl β -D-1-thiogalactopyranoside was added. Induced cultures were incubated 4 h at 37 °C (PDZ1, 2, 3) or overnight at 30 °C (PDZ1–2). Cells were harvested by spinning at 10000g for 10 min at 4 °C and resuspension in lysis buffer (50 mM Tris/HCL pH 7.5, 1 mM PMSF, 25 μ g/ml DNase, 40 mM Mg_2SO_4). The cells were destroyed using a cell disruptor apparatus at 26 KPsi. The cell lysate was spun down at 35000g for 1 h and the supernatant filtered with a 0.45 μ m and a 0.22 μ m filter. Purification was performed by first a nickel(II)-charged column (HisTrap HP, GE Healthcare, UK) equilibrated with Tris-buffer (Tris/HCl buffer 50 mM, pH 7.5) followed by anion-exchange chromatography for PDZ1 and 3 and gel-filtration for PDZ2 and 1–2. For anion-exchange chromatography, a MonoQ HR 5/5 column (GE Healthcare, UK) equilibrated with 50 mM Tris/HCL, pH 8.5, was used and elution was done with a gradient of 0–500 mM NaCl. For gel filtration, the PDZ sample was loaded on a Superdex 75 HR 10/30 column (GE Healthcare, UK) equilibrated with Tris buffer (20 mM Tris/HCL, pH 7.5) with a constant flow rate at 0.5 mL/min. The relevant fractions were analyzed on SDS-Page gel stained by a standard silver staining protocol. The final purification was analyzed by electrospray ionization liquid chromatography–mass spectrometry (ESI-LC/MS) to get the exact molecular weight and thereby verify the identity of the PDZ domain. Molar extinction coefficients were found by amino acids analysis (Alphalyse, Odense, Denmark) and thereafter used for measuring protein concentrations. For pull-down experiments, PDZ2 without His-tag was produced. For this, a slightly different construct was used that allowed the His-tag to be enzymatically cleaved off by bovine Thrombin (1 unit per 100 μ g protein; incubation overnight at room temperature while rotating), followed by purification using “reverse purification” on the HisTrap HP column under the same condition as previously described.

Fluorescence Polarization Assay. For measuring the binding affinity between the fluorescent peptides (Cy5–NR2B, 5-FAM–NR2B, Cy5–CRIPT, or 5-FAM–CRIPT) and PDZ saturation binding experiments were performed. To a fixed concentration of Cy5–NR2B, 5-FAM–NR2B, Cy5–CRIPT, or 5-FAM–CRIPT (50 nM) increasing concentrations of PDZ were added to get a saturation binding curve. The assay was performed in a 1 \times TBS buffer (150 mM NaCl, 10 mM Tris, pH 7.4) including 1% BSA in black flat-bottom 384-well plates (Corning Life Sciences, NY). After incubation for 20–30 min at room temperature, the FP of the samples was measured on a Safire² plate-reader (Tecan, Männedorf, Switzerland), but before reading the samples, the g-factor was adjusted for so that a 50 nM probe without any PDZ present would give a FP value of 20 mP. Cy5–NR2B and Cy5–CRIP, as well as 5-FAM–NR2B and 5-FAM–CRIPT were measured at excitation/emission values of 635/670 nm and 470/525 nm, respectively. The FP values were fitted to the equation $Y = B_{max} \times X / (K_d + X)$, with B_{max} being the maximal FP value, X is the PDZ concentration, and Y is variable FP values. As long as the concentration of labeled peptide is well below the true K_d during the assay, the K_d can be

directly derived from this saturation curve as being equal to the PDZ concentration where the curve is half-saturated (at these conditions $EC_{50} \equiv [total\ PDZ]_{half-saturation} = [free\ PDZ]_{half-saturation} \equiv K_d$).⁴² To measure the affinities between nonfluorescent peptides and PDZ domains, heterologous competition bindings assay were performed. This was done by adding increasing concentration of peptide to a fixed concentration of Cy5–NR2B, 5-FAM–NR2B, Cy5–CRIPT, or 5-FAM–CRIPT (50 nM) and PDZ (20 μ M for PDZ1, 3 μ M for PDZ2 and 1–2 and 5 μ M for PDZ3) in the same TBS buffer and conditions as described above. FP values were then fitted to the general equation: $Y = Bottom + (Top - Bottom) / [1 + (10^{(X - logIC_{50})})]$, where X is the logarithmic value of peptide concentration. Hereby the IC_{50} value was obtained, which is used to calculate the theoretical competitive inhibition constant, K_i .⁴²

Molecular Modeling. PDZ1 and PDZ2 were aligned with PDZ3 using Prime (Schrödinger, Portland, OR). From these sequences, homology models were created using the PDZ3 X-ray crystal structure (PDB structure 1BE9)²⁰ as template in Prime with standard parameters. The peptide ligand from 1BE9, KQTSV, was rebuilt to IESDV in the homology models. The side chains of the PDZ domain and the peptide were then minimized in Macromodel (Schrödinger, Portland, OR) using the force field OPLS2005 and by constraining the backbone. A grid around the peptide was generated in Glide (Schrödinger, Portland, OR) and used for docking. Relevant peptides were docked flexibly in Glide using default parameters, and the best scoring poses were energy minimized. The conserved water molecule seen in the binding pocket was kept constant during docking and minimization. Pymol, version 0.97, was used for creating figures.⁵²

Acknowledgment. This work was supported by the Lundbeck Foundation (K.S.), the Drug Research Academy, Faculty of Pharmaceutical Sciences, University of Copenhagen, Denmark (Ph.D. scholarship to A.B.), and the Swedish Research Council (P.J.). We thank Dr. Chris Armishaw for guidance on peptide synthesis and Julie K. Klint and Christine A. Ussing for assistance in the synthesis of peptides.

Supporting Information Available: Chemical structures of 5-FAM and Cy5-maleimide, experimental details, and results of the pull-down assay together with a table containing ESI-LC/MS data for compounds 1–39, 41–51, and 57. This material is available free of charge via the Internet at <http://pubs.acs.org>.

References

- (1) Arkin, M. R.; Wells, J. A. Small-molecule inhibitors of protein–protein interactions: progressing towards the dream. *Nat. Rev. Drug Discovery* **2004**, *3*, 301–317.
- (2) Ryan, D. P.; Matthews, J. M. Protein–protein interactions in human disease. *Curr. Opin. Struct. Biol.* **2005**, *15*, 441–446.
- (3) Juliano, R. L.; Astriab-Fisher, A.; Falke, D. Macromolecular therapeutics: emerging strategies for drug discovery in the postgenome era. *Mol. Interv.* **2001**, *1*, 40–53.
- (4) Berg, T. Modulation of protein–protein interactions with small organic molecules. *Angew. Chem., Int. Ed.* **2003**, *42*, 2462–2481.
- (5) DeLano, W. L. Unraveling hot spots in binding interfaces: progress and challenges. *Curr. Opin. Struct. Biol.* **2002**, *12*, 14–20.
- (6) Bogan, A. A.; Thorn, K. S. Anatomy of hot spots in protein interfaces. *J. Mol. Biol.* **1998**, *280*, 1–9.
- (7) Wells, J. A.; McClendon, C. L. Reaching for high-hanging fruit in drug discovery at protein–protein interfaces. *Nature* **2007**, *450*, 1001–1009.
- (8) Chene, P. Drugs targeting protein–protein interactions. *ChemMedChem* **2006**, *1*, 400–411.
- (9) Vassilev, L. T.; Vu, B. T.; Graves, B.; Carvajal, D.; Podlaski, F.; Filipovic, Z.; Kong, N.; Kammlott, U.; Lukacs, C.; Klein, C.; Fotouhi, N.; Liu, E. A. In vivo activation of the p53 pathway by small-molecule antagonists of MDM2. *Science* **2004**, *303*, 844–848.
- (10) Kim, E.; Sheng, M. PDZ domain proteins of synapses. *Nat. Rev. Neurosci.* **2004**, *5*, 771–781.
- (11) Sheng, M.; Sala, C. PDZ domains and the organization of supramolecular complexes. *Annu. Rev. Neurosci.* **2001**, *24*, 1–29.
- (12) Schultz, J.; Copley, R. R.; Doerks, T.; Ponting, C. P.; Bork, P. SMART: a web-based tool for the study of genetically mobile domains. *Nucleic Acids Res.* **2000**, *28*, 231–234.

- (13) Kornau, H. C.; Schenker, L. T.; Kennedy, M. B.; Seeburg, P. H. Domain interaction between NMDA receptor subunits and the postsynaptic density protein PSD-95. *Science* **1995**, *269*, 1737–1740.
- (14) Kim, E.; Niethammer, M.; Rothschild, A.; Jan, Y. N.; Sheng, M. Clustering of Shaker-type K⁺ channels by interaction with a family of membrane-associated guanylate kinases. *Nature* **1995**, *378*, 85–88.
- (15) Songyang, Z.; Fanning, A. S.; Fu, C.; Xu, J.; Marfatia, S. M.; Chishti, A. H.; Crompton, A.; Chan, A. C.; Anderson, J. M.; Cantley, L. C. Recognition of unique carboxyl-terminal motifs by distinct PDZ domains. *Science* **1997**, *275*, 73–77.
- (16) Wiedemann, U.; Boisguerin, P.; Leben, R.; Leitner, D.; Krause, G.; Moelling, K.; Volkmer-Engert, R.; Oschkinat, H. Quantification of PDZ domain specificity, prediction of ligand affinity and rational design of super-binding peptides. *J. Mol. Biol.* **2004**, *343*, 703–718.
- (17) Stiffler, M. A.; Chen, J. R.; Grantcharova, V. P.; Lei, Y.; Fuchs, D.; Allen, J. E.; Zaslavskaja, L. A.; MacBeath, G. PDZ domain binding selectivity is optimized across the mouse proteome. *Science* **2007**, *317*, 364–369.
- (18) Lim, I. A.; Hall, D. D.; Hell, J. W. Selectivity and promiscuity of the first and second PDZ domains of PSD-95 and synapse-associated protein 102. *J. Biol. Chem.* **2002**, *277*, 21697–21711.
- (19) Hung, A. Y.; Sheng, M. PDZ domains: structural modules for protein complex assembly. *J. Biol. Chem.* **2002**, *277*, 5699–5702.
- (20) Doyle, D. A.; Lee, A.; Lewis, J.; Kim, E.; Sheng, M.; MacKinnon, R. Crystal structures of a complexed and peptide-free membrane protein-binding domain: molecular basis of peptide recognition by PDZ. *Cell* **1996**, *85*, 1067–1076.
- (21) Remaut, H.; Waksman, G. Protein–protein interaction through β -strand addition. *Trends Biochem. Sci.* **2006**, *31*, 436–444.
- (22) Chi, C. N.; Engström, Å.; Gianni, S.; Larsson, M.; Jemth, P. Two conserved residues govern the salt and pH dependencies of the binding reaction of a PDZ domain. *J. Biol. Chem.* **2006**, *281*, 36811–36818.
- (23) Niethammer, M.; Kim, E.; Sheng, M. Interaction between the C terminus of NMDA receptor subunits and multiple members of the PSD-95 family of membrane-associated guanylate kinases. *J. Neurosci.* **1996**, *16*, 2157–2163.
- (24) Dingledine, R.; Borges, K.; Bowie, D.; Traynelis, S. F. The glutamate receptor ion channels. *Pharmacol. Rev.* **1999**, *51*, 7–61.
- (25) Gardoni, F.; Di Luca, M. New targets for pharmacological intervention in the glutamatergic synapse. *Eur. J. Pharmacol.* **2006**, *545*, 2–10.
- (26) Hoyte, L.; Barber, P. A.; Buchan, A. M.; Hill, M. D. The rise and fall of NMDA antagonists for ischemic stroke. *Curr. Mol. Med.* **2004**, *4*, 131–136.
- (27) Brenman, J. E.; Chao, D. S.; Gee, S. H.; McGee, A. W.; Craven, S. E.; Santillano, D. R.; Wu, Z.; Huang, F.; Xia, H.; Peters, M. F.; Froehner, S. C.; Brecht, D. S. Interaction of nitric oxide synthase with the postsynaptic density protein PSD-95 and α 1-syntrophin mediated by PDZ domains. *Cell* **1996**, *84*, 757–767.
- (28) Christopherson, K. S.; Hillier, B. J.; Lim, W. A.; Brecht, D. S. PSD-95 assembles a ternary complex with the N-methyl-D-aspartic acid receptor and a bivalent neuronal NO synthase PDZ domain. *J. Biol. Chem.* **1999**, *274*, 27467–27473.
- (29) Aarts, M.; Liu, Y.; Liu, L.; Besshoh, S.; Arundine, M.; Gurd, J. W.; Wang, Y. T.; Salter, M. W.; Tymianski, M. Treatment of ischemic brain damage by perturbing NMDA receptor–PSD-95 protein interactions. *Science* **2002**, *298*, 846–850.
- (30) Aarts, M. M.; Tymianski, M. Novel treatment of excitotoxicity: targeted disruption of intracellular signalling from glutamate receptors. *Biochem. Pharmacol.* **2003**, *66*, 877–886.
- (31) Cui, H.; Hayashi, A.; Sun, H. S.; Belmares, M. P.; Cobey, C.; Phan, T.; Schweizer, J.; Salter, M. W.; Wang, Y. T.; Tasker, R. A.; Garman, D.; Rabinowitz, J.; Lu, P. S.; Tymianski, M. PDZ protein interactions underlying NMDA receptor-mediated excitotoxicity and neuroprotection by PSD-95 inhibitors. *J. Neurosci.* **2007**, *27*, 9901–9915.
- (32) Thomson Current Drugs; <http://www.thomson.com>.
- (33) Hajduk, P. J.; Huth, J. R.; Fesik, S. W. Druggability indices for protein targets derived from NMR-based screening data. *J. Med. Chem.* **2005**, *48*, 2518–2525.
- (34) Wen, W.; Wang, W.; Zhang, M. Targeting PDZ domain proteins for treating NMDA receptor-mediated excitotoxicity. *Curr. Top. Med. Chem.* **2006**, *6*, 711721.
- (35) Joshi, M.; Vargas, C.; Boisguerin, P.; Diehl, A.; Krause, G.; Schmieder, P.; Moelling, K.; Hagen, V.; Schade, M.; Oschkinat, H. Discovery of low-molecular-weight ligands for the AF6 PDZ domain. *Angew. Chem., Int. Ed.* **2006**, *45*, 3790–3795.
- (36) Hammond, M. C.; Harris, B. Z.; Lim, W. A.; Bartlett, P. A. β -Strand peptidomimetics as potent PDZ domain ligands. *Chem. Biol.* **2006**, *13*, 1247–1251.
- (37) Fujii, N.; Haresco, J. J.; Novak, K. A.; Stokoe, D.; Kuntz, I. D.; Guy, R. K. A selective irreversible inhibitor targeting a PDZ protein interaction domain. *J. Am. Chem. Soc.* **2003**, *125*, 12074–12075.
- (38) Fujii, N.; Haresco, J. J.; Novak, K. A.; Gage, R. M.; Pedemonte, N.; Stokoe, D.; Kuntz, I. D.; Guy, R. K. Rational design of a nonpeptide general chemical scaffold for reversible inhibition of PDZ domain interactions. *Bioorg. Med. Chem. Lett.* **2007**, *17*, 549–552.
- (39) Mayasundari, A.; Ferreira, A. M.; He, L.; Mahindroo, N.; Bashford, D.; Fujii, N. Rational design of the first small-molecule antagonists of NHERF1/EBP50 PDZ domains. *Bioorg. Med. Chem. Lett.* **2008**, *18*, 942–945.
- (40) Piserchio, A.; Salinas, G. D.; Li, T.; Marshall, J.; Spaller, M. R.; Mierke, D. F. Targeting specific PDZ domains of PSD-95; structural basis for enhanced affinity and enzymatic stability of a cyclic peptide. *Chem. Biol.* **2004**, *11*, 469–473.
- (41) Fry, D. C.; Vassilev, L. T. Targeting protein–protein interactions for cancer therapy. *J. Mol. Med.* **2005**, *83*, 955–963.
- (42) Nikolovska-Coleska, Z.; Wang, R.; Fang, X.; Pan, H.; Tomita, Y.; Li, P.; Roller, P. P.; Krajewski, K.; Saito, N. G.; Stuckey, J. A.; Wang, S. Development and optimization of a binding assay for the XIAP BIR3 domain using fluorescence polarization. *Anal. Biochem.* **2004**, *332*, 261–273.
- (43) Chi, C. N.; Gianni, S.; Calosci, N.; Travaglini-Allocatelli, C.; Engström, Å.; Jemth, P. A conserved folding mechanism for PDZ domains. *FEBS Lett.* **2007**, *581*, 1109–1113.
- (44) Gianni, S.; Engström, Å.; Larsson, M.; Calosci, N.; Malatesta, F.; Eklund, L.; Ngang, C. C.; Travaglini-Allocatelli, C.; Jemth, P. The kinetics of PDZ domain–ligand interactions and implications for the binding mechanism. *J. Biol. Chem.* **2005**, *280*, 34805–34812.
- (45) Saro, D.; Li, T.; Rupasinghe, C.; Paredes, A.; Caspers, N.; Spaller, M. R. A thermodynamic ligand binding study of the third PDZ domain (PDZ3) from the mammalian neuronal protein PSD-95. *Biochemistry* **2007**, *46*, 6340–6352.
- (46) Harris, B. Z.; Lau, F. W.; Fujii, N.; Guy, R. K.; Lim, W. A. Role of electrostatic interactions in PDZ domain ligand recognition. *Biochemistry* **2003**, *42*, 2797–2805.
- (47) Niethammer, M.; Valtschanoff, J. G.; Kapoor, T. M.; Allison, D. W.; Weinberg, R. J.; Craig, A. M.; Sheng, M. CRIPT, a novel postsynaptic protein that binds to the third PDZ domain of PSD-95/SAP90. *Neuron* **1998**, *20*, 693–707.
- (48) Hruby, V. J. Designing peptide receptor agonists and antagonists. *Nat. Rev. Drug Discovery* **2002**, *1*, 847–858.
- (49) Karthikeyan, S.; Leung, T.; Ladias, J. A. Structural basis of the Na⁺/H⁺ exchanger regulatory factor PDZ1 interaction with the carboxyl-terminal region of the cystic fibrosis transmembrane conductance regulator. *J. Biol. Chem.* **2001**, *276*, 19683–19686.
- (50) Fukuyama, T.; Jow, C.-K.; Mui, C. 2- and 4-Nitrobenzenesulfonamides: exceptionally versatile means for preparation of secondary amines and protection of amines. *Tetrahedron Lett.* **1995**, *36*, 6373–6374.
- (51) Yang, L.; Chiu, K. Solid phase synthesis of Fmoc N-methyl amino acids: application of the Fukuyama amine synthesis. *Tetrahedron Lett.* **1997**, *38*, 7307–7310.
- (52) DeLano, W. L. The PyMOL Molecular Graphics System on World Wide Web; <http://www.pymol.org>.